



# Molecular dynamics simulation of vaporization of an ultra-thin liquid argon layer on a surface

Pan Yi <sup>a</sup>, D. Poulikakos <sup>a,\*</sup>, J. Walther <sup>b</sup>, G. Yadigaroglu <sup>c</sup>

<sup>a</sup> *Laboratory of Thermodynamics in Emerging technologies, Institute of Energy Technology, Swiss Federal Institute of Technology, ETH-Zentrum, CH-8092 Zurich, Switzerland*

<sup>b</sup> *Department of Information Sciences, Institute of Computational Sciences, Swiss Federal Institute of Technology, ETH-Zentrum, CH-8092 Zurich, Switzerland*

<sup>c</sup> *Nuclear Engineering Laboratory, Institute of Energy Technology, Swiss Federal Institute of Technology, ETH-Zentrum, CH-8092 Zurich, Switzerland*

Received 8 December 2000; received in revised form 14 August 2001

---

## Abstract

We performed molecular dynamics simulations of the vaporization phenomenon of an ultra-thin layer (2 nm) of liquid argon on a platinum surface. The simulation started from a molecular system of three phases (liquid argon, solid platinum and argon vapor) in equilibrium at 110 K. The platinum wall was then suddenly heated to a higher temperature (a moderately higher temperature of 150 K and a much higher temperature of 300 K were investigated). Features of our simulation model include a fast algorithm based on a tree data structure and a constant temperature solid wall model based on a 3-D Langevin equation. The entire vaporization process was successfully simulated. The results reveal trends that agree with our knowledge of vaporization of a similar macroscopic system. For example, for the high surface temperature the vaporization process is reminiscent of the Leidenfrost phenomenon and after the formation of a vapor region between the surface and the liquid mass, the latter deforms and tends to approximately acquire a spherical “droplet” shape, as one would have expected from macroscopic considerations. Contrary to this, a gradual evaporation process occurs at moderate wall temperatures. After complete evaporation and upon reduction of the wall temperature, condensation takes place leading to reconstruction of the initial liquid layer. © 2002 Elsevier Science Ltd. All rights reserved.

*Keywords:* Boiling; Molecular dynamics; Nanoscale

---

## 1. Introduction

The phenomenon of early stage vapor formation in a liquid mass in contact with a hot surface has been investigated both theoretically and experimentally at the macroscopic (continuum) level for many years, relying on scientifically logical but largely heuristic arguments for the initiation of vapor nucleation. Research on the same phenomenon at the molecular level is by compar-

ison scarce, despite the obvious need for such research in order to circumvent the limitations of empirical assumptions that are unavoidable in the macroscopic approach. This situation arises from two reasons. One is that experimental research under such small time (ps) and space (nm) scales still faces today formidable instrumentation difficulties. The other reason is that in theoretical/numerical research the usual macroscopic continuum models no longer describe the vaporization phenomenon at such small scales; new alternative models accounting explicitly for intermolecular interactions need to be found.

One promising approach is Molecular Dynamics Simulation (MDS). In this approach, one goes directly to the molecular level. By solving Newton's equation of

---

\* Corresponding author. Tel.: +41-1-632-2738; fax: +41-1-632-1176.

*E-mail address:* poulikakos@lntn.iet.mavt.ethz.ch (D. Poulikakos).

Nomenclature	
$a$	acceleration
$c$	coefficient in the Verlet algorithm for 3D Langevin equation
$c_{rv}$	correlation coefficient
$f$	interaction force between atoms
$F$	random force
$\mathbf{F}$	force vector
$k_B$	Boltzmann constant
$m$	mass
$N$	number of atoms in the simulation domain
$\mathbf{p}$	momentum vector
$\mathbf{r}$	position
$\mathbf{r}$	position vector
$r_c$	cut-off distance
$\delta r^G$	random variable sampled from a bivariate Gaussian distribution
$t$	time
$\delta t$	time step of simulation
$u$	potential
$v$	velocity
$\mathbf{v}$	velocity vector
$\delta v^G$	random variable sampled from a bivariate Gaussian distribution
<i>Greek symbols</i>	
$\varepsilon$	energy parameter in potential function
$\xi$	damper force constant
$\rho$	joint probability density function
$\sigma$	length parameter in potential function
$\sigma_r$	variance of a bivariate Gaussian distribution
$\sigma_v$	variance of a bivariate Gaussian distribution
$\phi$	potential function
<i>Subscripts</i>	
0, 1, 2	index
c	cut-off
$i$	the $i$ th
$j$	the $j$ th
r	related to position
v	related to velocity
<i>Superscript</i>	
G	related to Gaussian distribution

motion of every molecule in the system of interest numerically, detailed information on the entire microscopic system can be obtained. Although this idea is not new (it dates back to the 1950s and 1960s, when some pioneering investigations were performed in the field of theoretical physics), it is not until recently that its employment in relatively large systems has begun. To exemplify early studies, in 1957, Alder and Wainwright [1] studied the phase transitions in a hard sphere system of particles (perfectly elastic collisions). In 1964, Rahman [2] successfully solved the equations of motion for a set of Lennard–Jones particles. In selected engineering systems, the MDS method can provide information that allows the revision or verification of ad hoc assumptions of continuum theory. However, there are two formidable difficulties that need to be overcome: first, all relevant intermolecular interactions should be correctly accounted for, and second, a large number of molecules need to be simulated in order to bridge the gap between the molecular and the continuum levels and provide closure information for macroscopic models, or aid the understanding of the physics of the phenomena of interest.

With reference to phase change, Long et al. [3] and Little [4] studied the evaporation of a liquid argon droplet exposed to both subcritical and supercritical surroundings using 5600 atoms, 27,000 atoms and 100,000 atoms. The evaporation rate obtained by MDS agrees well with existing theoretical results. Maruyama and Kimura [5] simulated the heterogeneous nucleation

of a vapor bubble on a solid surface. The formation of a bubble on the surface was clearly visualized and the contact angle obtained was in good agreement with former studies.

In the present paper, employing the MDS method, we simulated the vaporization of a thin liquid argon film on a suddenly heated platinum surface. The reason for this choice is that the molecular description of these materials is both quite well known and in comparison to other even more complex materials, tractable. The results reveal interesting trends that are reminiscent of macroscopic phenomena such as the Leidenfrost phenomenon at high wall temperatures and the tendency of a liquid droplet to attain a spherical shape corresponding to an energy minimum. Reduction of the wall temperature gives rise to condensation and the reconstruction of the evaporated liquid layer.

## 2. On the molecular dynamics simulation method

The premise of MDS can be described as follows: considering the fact that at the primitive level every substance is made from elementary particles (atoms or molecules), if the basic dynamics parameters of these molecules, i.e. position, velocity, and interaction force, can be determined, the macroscopic physical properties of the substance, like volume, temperature, pressure, etc. can subsequently be obtained via statistical methods. Based on this idea, the starting point of MDS is

Newton's second law. For the translational motion of a spherically symmetric molecule, this law has the simple form

$$\mathbf{F} = m \frac{d^2 \mathbf{r}}{dt^2}, \quad (1)$$

where  $\mathbf{F}$  is the sum of the forces exerted on the molecule by the other molecules in the system,  $\mathbf{r}$  is the position vector of the molecule,  $t$  is the time, and  $m$  is the mass of the molecule.

Integrating Eq. (1) once in time yields the velocity of the molecule. Integrating once more results in its displacement. If one integrates Eq. (1) for every molecule in the simulation domain step by step from some initial state, then detailed information of the movement of every molecule is obtained. This information can be further processed by time averaging, space averaging or both to provide the macroscopic physical properties over the entire simulation domain.

For molecules that have internal complex geometry, the original simple Newton equation of motion is no longer sufficient. Depending on the type of molecular model used, a generalized form of the original Newton equation is adopted in the simulations. For example, using a rigid-body model, one has to consider the rotation of the molecule around its mass center; therefore the so-called "Euler Equation" should be used. However, no matter how complex the form of the equation of motion, the basic simulation procedure is always the same: first, integrating the equation of motion of every molecule to acquire its dynamical parameters; then performing an averaging of these dynamical parameters to obtain the values of macroscopic physical properties.

In the above discussion, nothing has been said about the form and magnitude of the force term in the left-hand side of Eq. (1). In fact, this is one of the core problems in molecular dynamics. To calculate the interaction force among molecules, since this force is electric/electromagnetic in nature, one needs to decide on an appropriate corresponding intermolecular potential model. Usually this model comes from experimental data or quantum mechanics calculations and accounts for the contribution from two-body and three-body potentials. For calculations in a group of molecules, a many-body potential needs to be used. Due to their small contribution to the total potential (and their significant effect on computational speed), the effect of more than two or three bodies in the potential equation is either safely overlooked or simply appears as a correction term in the potential equation that can be calculated easily [6]. In most practical simulations, researchers even simplified the potential model further to consider only two-body potential so as to shorten the computation time with acceptable accuracy. Normally this is done by defining an "effective pair potential" and

incorporating the effect of a three-body potential into this effective pair potential [6].

When a two-body potential model is chosen, the interaction force between a pair of molecules can be derived from this potential by the following relation:

$$\mathbf{F}_{ij} = -\nabla u_{ij}, \quad (2)$$

where  $\mathbf{F}_{ij}$  is the force acting on the  $i$ th molecule by the  $j$ th molecule,  $u_{ij}$  is the two-body potential between the  $i$ th molecule and the  $j$ th molecule.

Summing up all the forces exerted on one molecule by other molecules yields the total force on this molecule. After the total force on every molecule in the simulation domain has been calculated, one can integrate Eq. (1) in time for each molecule.

### 3. Computational model

The simulation domain we selected for the problem of interest is a cuboid, which is composed of two regions (Fig. 1): the solid wall (represented by the triangles) and the "fluid" region (represented by the circles). Three layers of Pt atoms lie at the bottom of the simulation domain and form the solid wall. The interaction force among the Pt atoms is a harmonic force (spring force). Their spatial arrangement follows the fcc(1 1 1) crystal lattice. The distance between neighboring molecules is  $2.77 \times 10^{-10}$  m and the spring force constant is 46.8 N/m [5] (Figs. 2 and 3). Right above the solid wall is the fluid region, which is fully occupied by argon molecules. The potential between a pair of argon molecules is described by the function suggested by Stoddard and Ford [8], which features a shift for the continuous decay

$$\phi(r) = 4\epsilon \left[ \left\{ \left( \frac{\sigma}{r} \right)^{12} - \left( \frac{\sigma}{r} \right)^6 \right\} + \left\{ 6 \left( \frac{\sigma}{r_c} \right)^{12} - 3 \left( \frac{\sigma}{r_c} \right)^6 \right\} \left( \frac{r}{r_c} \right)^2 - \left\{ 7 \left( \frac{\sigma}{r_c} \right)^{12} - 4 \left( \frac{\sigma}{r_c} \right)^6 \right\} \right], \quad (3)$$

where  $\sigma = 3.40 \times 10^{-10}$  m and  $\epsilon = 1.67 \times 10^{-21}$  J. The cut-off distance  $r_c$  is set at  $3.5\sigma$ . For the interaction between Pt and argon particles, we employ the same form of potential function as above, but the values of the  $\sigma$  and  $\epsilon$  parameters have been changed to  $3.085 \times 10^{-10}$  m and  $0.894 \times 10^{-21}$  J, respectively, according to the suggestions of Maruyama and Kimura [5].

The upper boundary of the computational domain is an imaginary perfectly adiabatic "wall". The collision of an atom with this boundary is purely elastic. The distance of this wall from the platinum surface is selected to be large enough so that the evaporation process is not affected.

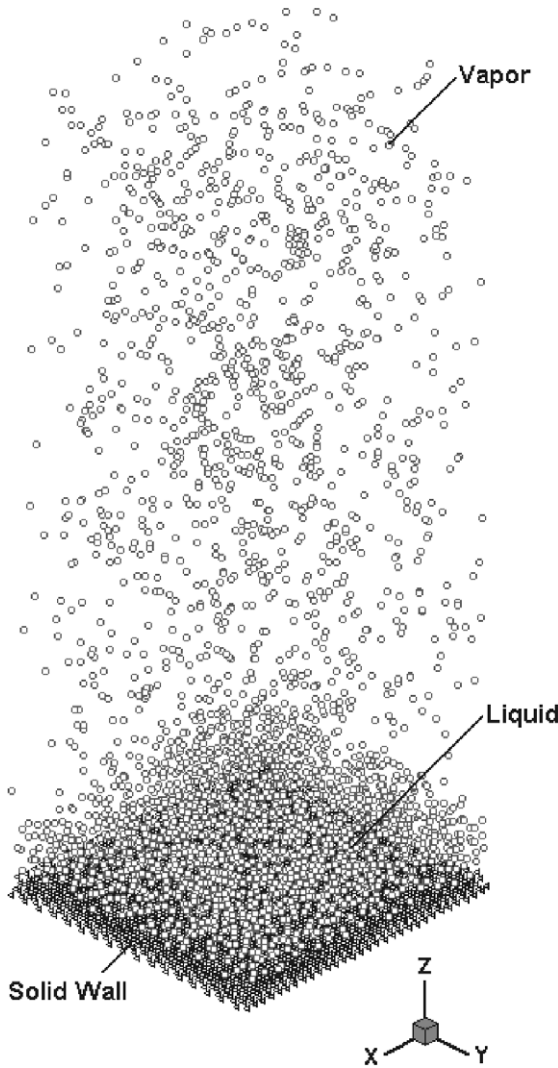


Fig. 1. Simulation domain.

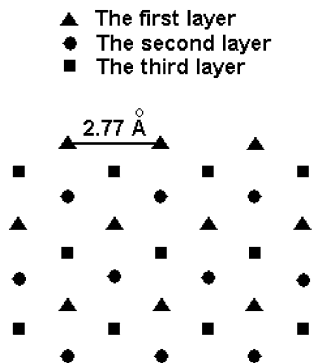


Fig. 2. Top view of the lattice of wall molecules fcc(111).

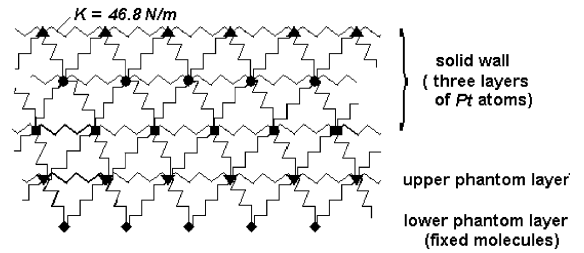


Fig. 3. Solid wall and phantom layers (projection in the  $y$ - $z$  plane).

For controlling the temperature of the solid wall, we inserted another two layers of Pt atoms right below the lowest layer of Pt atoms. These two “phantom layers” do not interact with argon atoms. The spatial arrangement of the two phantom layers still follows the fcc(111) structure, as if they were just a natural extension of the crystal lattice (Fig. 3). The lower phantom layer of Pt atoms is fixed to the crystal lattice at all times during the simulation. Two extra forces, a damper force and a random force, are exclusively imposed on the Pt atoms of the upper phantom layer (right below the lowest real layer). With these two extra forces (appropriately selected) the long-term dynamical behavior of the upper phantom layer conforms to the 3D Langevin equation (Section 4 of this paper presents a detailed description of this equation), which guarantees that both the temperature of this layer and the temperature of the solid wall stay constant if thermal equilibrium between them is reached. For the other four vertical boundaries, periodic boundary conditions were adopted.

#### 4. Algorithms

For the integration of the Newton equation for the molecules in the computation domain, we employ the “velocity Verlet” algorithm [6], which takes the following form:

$$r(t + \delta t) = r(t) + \delta t v(t) + \frac{1}{2} \delta t^2 a(t), \tag{4a}$$

$$v(t + \delta t) = v(t) + \frac{1}{2} \delta t [a(t) + a(t + \delta t)], \tag{4b}$$

where  $r$  is the position vector of an atom,  $v$  is the velocity vector of an atom,  $\delta t$  is time step of simulation, and  $a$  is the acceleration of an atom.

To perform the calculation of the interaction forces between atoms efficiently, we adopted a tree data structure in our program [7]. We subdivided the 3D computational domain into eight small equal-sized cubic cells recurrently (Fig. 4 illustrates such a subdivision of a 2D computational domain). Several levels

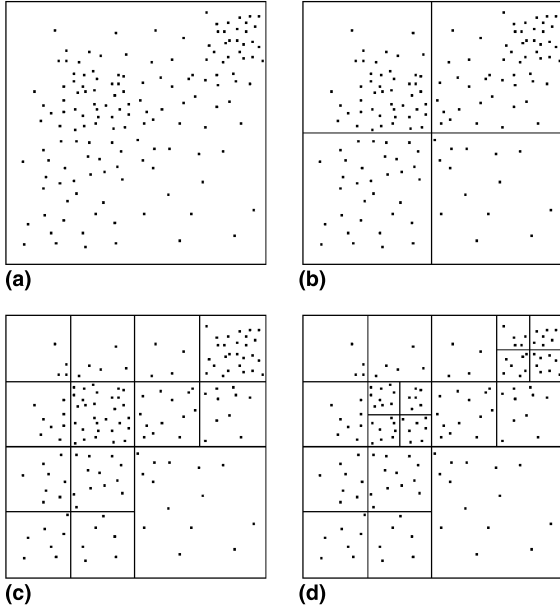


Fig. 4. Step-by-step subdivision of the space for a simple 2D particle distribution and resulting tree levels: (a) Step-1; (b) Step 2; (c) Step 3; (d) Step 4.

of the resulting tree are shown. This subdivision is terminated when either of the following two criteria is fulfilled:

- the cell size is smaller than the cut-off distance in the potential equation,
  - the number of particles in a cell is less than 20.
- Here the selection of number “20” reflects a balance between the computational time spent on constructing the tree structure and the computational time saved by employing the tree structure.

After the subdivision is completed, we construct a tree data structure by marching from the highest level (the entire computational domain) to the lowest level. The cells at the positions of the “leaves” of this “tree” structure are named “childless cells”. The next step is to find the near neighbors of a childless cell, i.e. cells that lie within the cut-off distance from the border of a childless cell. When all the near neighbors of a childless cell are found, the interaction force calculation can be performed directly. The advantage of the algorithm based on a tree data structure is that it can greatly reduce the interaction force computation time from order of  $O(N^2)$  to order of  $O(N \log N)$  (here  $N$  represents the number of atoms in the simulation domain) [7]. In large simulations, this algorithm is especially efficient and economical compared to a “normal” algorithm.

For the integration of the equations of motion of the molecules in the upper phantom layer, that has a different physical model, we employed the Verlet algorithm

corresponding to the 3D Langevin equation. As mentioned above, two extra forces, a damper force and a random force were imposed *only on the atoms of the upper phantom layer*, so that the equation of motion of these atoms (3D Langevin equation) has the following form [6]:

$$\frac{dp_i(t)}{dt} = -\xi p_i(t) + f(t) + F(t), \quad (5)$$

where  $p_i(t)$  is the momentum vector of the  $i$ th atom in the upper phantom layer;  $\xi$  is the damper force constant,  $f(t)$  is the interaction force between the  $i$ th atom and other atoms,  $F(t)$  is a random force which is sampled from a Gaussian distribution with zero mean value and a standard deviation given by  $\sigma = \sqrt{2\xi k_B T / \delta t}$ , where  $T$  is the preset target temperature value corresponding to the thermal equilibrium state),  $\delta t$  is the time step of simulation, and  $k_B$  is the Boltzman constant.

The 3D Langevin equation above is then integrated with the following Verlet algorithm [6]:

$$r(t + \delta t) = r(t) + c_1 \delta t v(t) + c_2 \delta t^2 a(t) + \delta r^G, \quad (6a)$$

$$v(t + \delta t) = c_0 v(t) + (c_1 - c_2) \delta t a(t) + c_2 \delta t a(t + \delta t) + \delta v^G. \quad (6b)$$

The values of  $c_0$ ,  $c_1$ , and  $c_2$  are determined by the following relations:

$$\begin{aligned} c_0 &= e^{-\xi \delta t}, & c_1 &= (\xi \delta t)^{-1} (1 - c_0), \\ c_2 &= (\xi \delta t)^{-1} (1 - c_1) \end{aligned} \quad (7)$$

$\delta v^G$  and  $\delta r^G$  are two values sampled from a bivariate Gaussian distribution which is described by a joint probability density function  $\rho$  [6]

$$\begin{aligned} &\rho(\delta r^G, \delta v^G) \\ &= \frac{1}{2\pi\sigma_r\sigma_v(1-c_{rv}^2)^{1/2}} \exp \left\{ -\frac{1}{2(1-c_{rv}^2)} \left( \left( \frac{\delta r^G}{\sigma_r} \right)^2 \right. \right. \\ &\quad \left. \left. + \left( \frac{\delta v^G}{\sigma_v} \right)^2 - 2c_{rv} \left( \frac{\delta r^G}{\sigma_r} \right) \left( \frac{\delta v^G}{\sigma_v} \right) \right) \right\} \end{aligned} \quad (8)$$

with zero mean values and variance given by

$$\begin{aligned} \sigma_r^2 &= \delta t^2 \frac{k_B T}{m} (\xi \delta t)^{-1} (2 - (\xi \delta t)^{-1} (3 - 4e^{-\xi \delta t} \\ &\quad + e^{-2\xi \delta t})), \end{aligned} \quad (9a)$$

$$\sigma_v^2 = \frac{k_B T}{m} (1 - e^{-2\xi \delta t}). \quad (9b)$$

The correlation coefficient  $c_{rv}$  is determined by

$$c_{rv} \sigma_r \sigma_v = \frac{k_B T}{m \xi} (1 - e^{-\xi \delta t})^2. \quad (10)$$

The above process controls the platinum wall temperature to a desired value.

## 5. Simulation procedure, results and discussion

The simulation process follows a three-step procedure. The first step is to achieve thermal equilibrium of all the phases in the domain (solid wall, liquid argon and argon vapor). This step can be further divided into two sub-steps: a velocity-scaling period and a period without velocity scaling. During the velocity-scaling period, the velocities of the molecules in each phase are scaled at every time step so as to keep the temperature of each phase at a constant value. After a sufficiently long time, the velocity scaling is switched off. The molecules then move freely until finally thermal equilibrium of all the phases is reached.

The second step of the simulation solely applies to the solid molecules. In this step, we isolate the solid wall from the computational domain and “heat” it to a high temperature as described below. When thermal equilibrium between the real wall and the phantom layer is reached, we proceed to the third step. In this step, the “hot” wall is reinserted into the computational domain and replaces the “cold” wall of the first step.

We first simulated the vaporization of a layer with a relatively small number of atoms. The computational domain was 8.31 nm (long)  $\times$  8.156 nm (deep normal to the paper)  $\times$  23.27 nm (tall). The number of argon and Pt atoms was 3186 and 3060, respectively. Each additional phantom layer contains 1020 Pt atoms. According to the recommendation of Tully [9], the  $\zeta$  parameter in the Langevin equation is set to the value of  $1.613 \times 10^{13}$  1/s. The time step is 1 fs. At the first stage of our simulation, we set the equilibrium temperature of the entire system to 110 K. At this temperature, a thin layer of liquid argon (about 2 nm in thickness) is placed above the wall. The presence of the surface tension aids the stabilization of the liquid/vapor interface. On top of this liquid layer there exists a thicker layer of argon vapor, which is about 20 nm in thickness. When the entire system reaches thermal equilibrium, the Platinum wall is isolated from the computational domain as noted above. By adjusting the parameters in Langevin equation, this wall is “heated” to a desirable temperature by the phantom layers. At the third stage of simulation, this hot wall is reinserted into the system to heat the argon fluid starting from the initial equilibrium temperature of 110 K. The vaporization of liquid argon then takes place and continues until thermal equilibrium at the wall temperature is reached again.

### 5.1. High temperature case

Fig. 5 illustrates the history of the average temperatures of the wall and argon regions, respectively. From 0 to 1000 ps, the simulation domain is in equilibrium state at 110 K. Then the wall molecules (and phantom molecules) are “removed” from the simulation domain to be

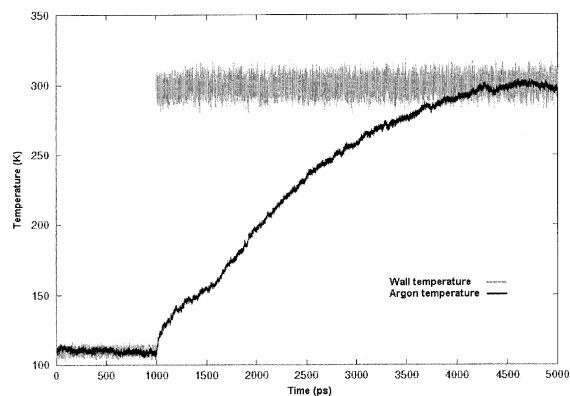


Fig. 5. Temperature history of the wall and argon regions – high temperature case 300 K.

heated separately; the wall is heated to 300 K and reaches thermal equilibrium with the phantom layers. This process lasts 500 ps (this time period is not shown in Fig. 5 and not counted in the total time). The “hot” wall is reinserted into the simulation immediately after the heating. The evaporation of the thin layer of liquid argon starts at 1000 ps and finishes at 5000 ps when thermal equilibrium between argon and wall is reached. Although it takes 4000 ps for the simulation domain to migrate from one established thermal equilibrium state to a new thermal equilibrium state, the actual evaporation of the liquid argon layer lasts only about 600 ps.

Fig. 6 shows a projection of the entire simulation domain in the  $y$ - $z$  plane at representative simulation times. In these pictures, the middle-size white dots (at the bottom of each picture) represent wall molecules, while the small and large white dots represent argon molecules in the gas and liquid phases, respectively. The argon molecules that are in the liquid phase are determined by calculating the local number density. We set a threshold radius of 0.5 nm and a threshold number density of 5, which corresponds to the average density at the phase interface of a mixed system of argon vapor and liquid at 110 K [10]. For every argon atom in the simulation domain, a sphere is drawn with its center at that atom and its radius being equal to the threshold radius mentioned earlier. We then count the argon molecules inside this sphere. If the number exceeds or equals the threshold number density, the argon molecule at the center of the sphere is determined to be in the liquid phase.

As can be seen in Fig. 6, at the beginning of the process, two phase interfaces, i.e. the interface between liquid argon and gas argon and the interface between liquid argon and solid wall, are clearly visible (Fig. 6(a)). In Fig. 6(b), small regions of vapor begin to appear at the wall neighborhood and the liquid region on the wall becomes discontinuous. The phase interface between the

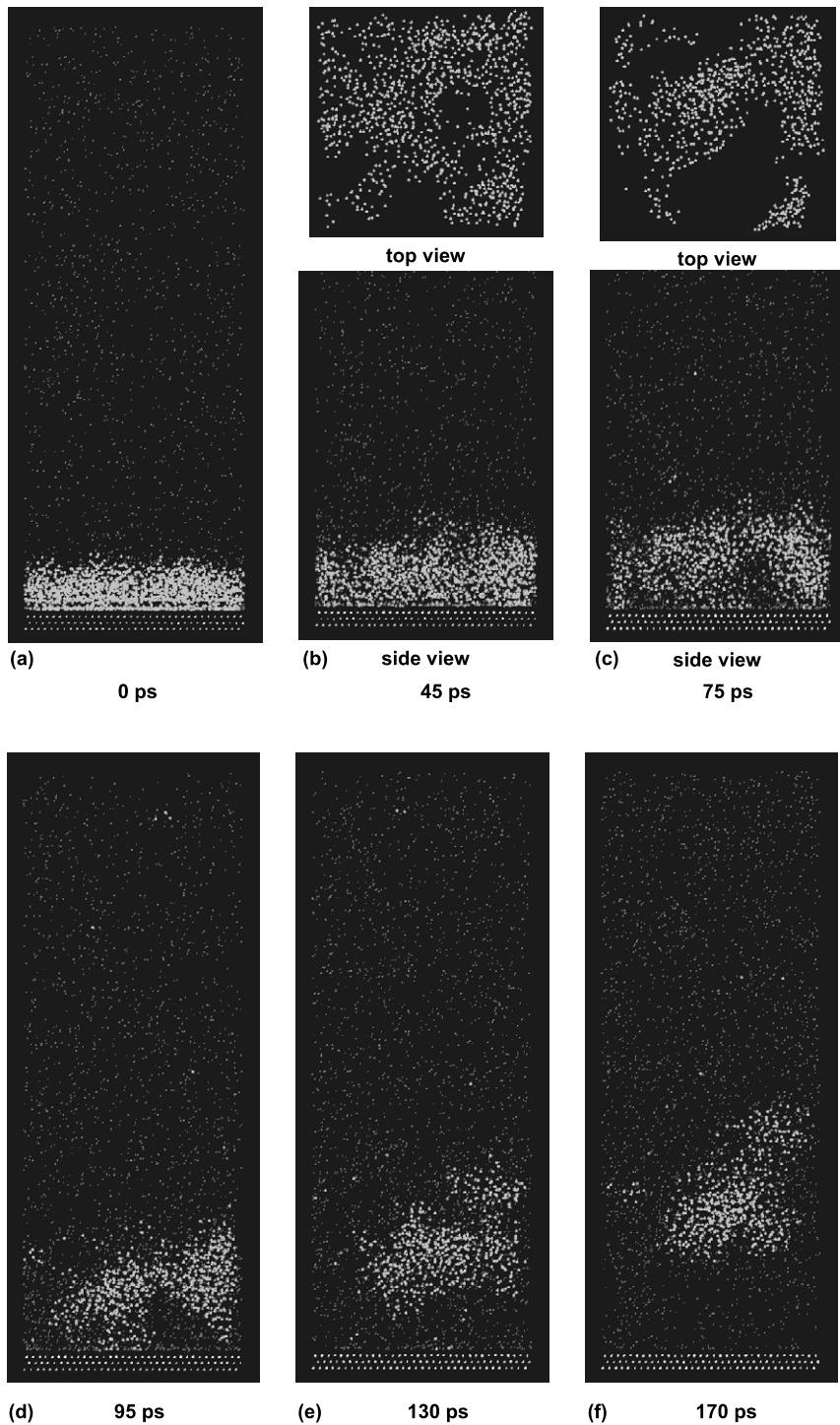


Fig. 6. Projection of the simulation domain in the  $y$ - $z$  plane at characteristic times – high temperature case 300 K.

bulk liquid and gas regions also becomes distorted. In Fig. 6(c), a relatively distinct vapor region can be seen forming on the wall surface and the liquid-occupied

portion of the wall surface decreases further. In Fig. 6(d), almost all the wall surface is covered by argon vapor and the bulk region of liquid argon floats on top

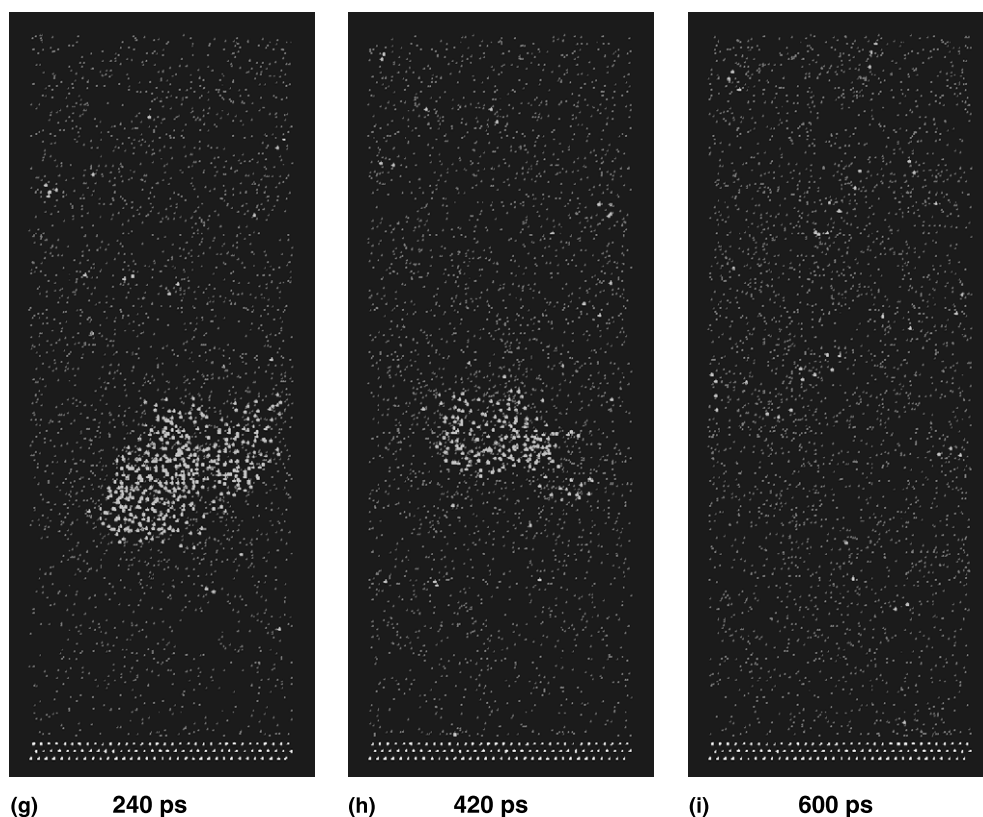


Fig. 6. (Continued)

of a vapor layer in a manner reminiscent of the Leidenfrost phenomenon. The liquid argon region continues to be pushed upwards and changes its shape in Figs 6(e)–(h) approaching a spherical shape, until it evaporates completely (Fig. 6(i)) 600 ps after heating of the wall.

The number-density profile in the  $Z$  direction (normal to the wall) as a function of time after wall heatup is shown in Fig. 7. The distance between the wall surface and the upper boundary of the computational domain is divided into eighty equal slices. The number of argon molecules in each slice is then counted to obtain the average number density of each slice. By observing the number density variation, we can draw two conclusions. First, the fact that the number density curves gradually flatten out illustrates the gradual disappearance of the gas-liquid phase interface. In fact the entire ultrathin liquid region can be characterized as a phase transition region. Second, the position of liquid argon can be identified immediately by locating the regions of the density peaks appearing in the curves of Fig. 7. The floating liquid containing zone is for example clearly visible in Fig. 7(c) between 7 and 12 nm away from the wall.

### 5.2. Low temperature case

We subsequently investigated another case in which the initial temperature difference between the hot wall and the argon regions was more moderate. Fig. 8 illustrates the temperature history curve. Again, the simulation domain was initially at equilibrium from 0 to 1000 ps at 110 K. The wall was then heated to 150 K. The evaporation procedure lasted now about 1500 ps, which is at a sharp contrast with the 600 ps of the former case.

Similar to Fig. 6, Fig. 9 shows the projection of the entire simulation domain in the  $y$ - $z$  plane at representative times of the simulation. In the following discussion in Figs. 9 and 10, we refer to the times after the wall heat up. We can see from this set of pictures that up to at least 300 ps after heating, the wall remains almost completely wetted although some parts of the wall surface may be temporarily occupied by small patches of vapor. On the other hand, the interface between bulk liquid and gas regions experiences a marked distortion: at 300 ps three peaks of liquid argon form above the initially flat liquid-gas interface. In order to aid the discussion with better visualization, in Figs. 9(d)–(f) *top*



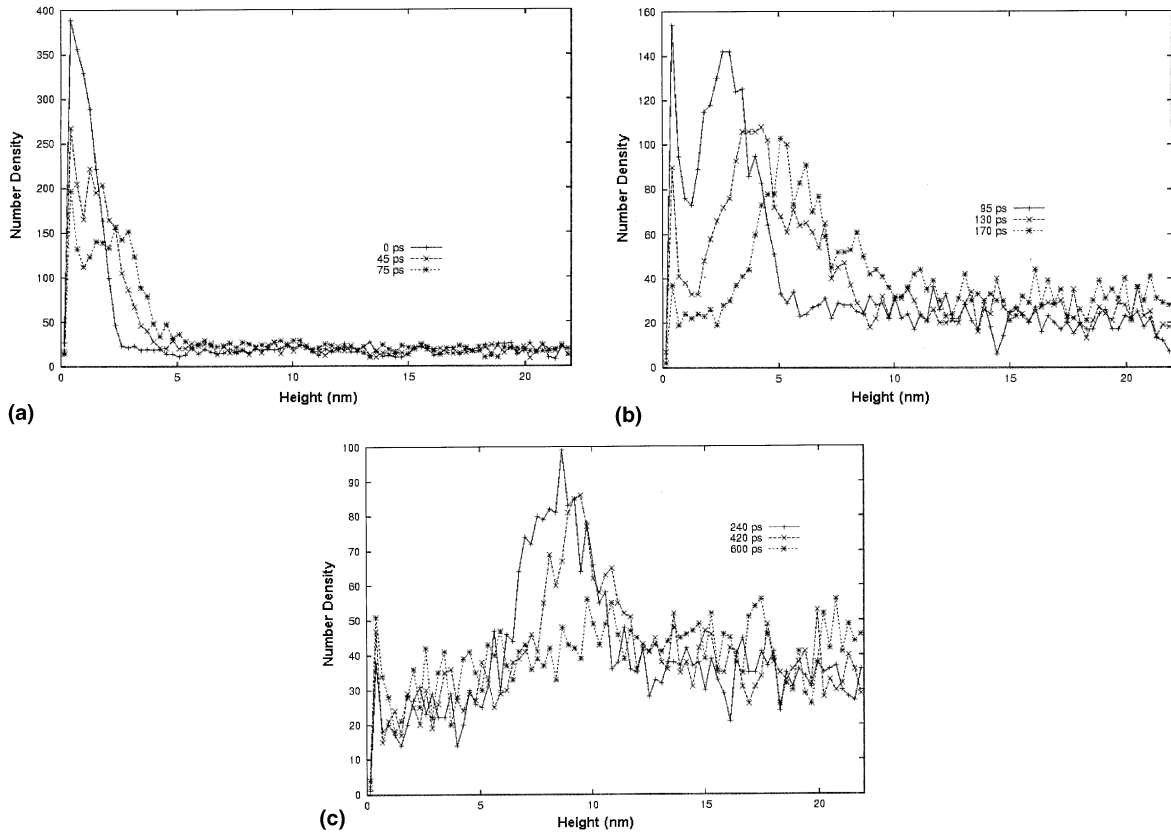


Fig. 7. Number density profiles at different times regions – high temperature case 300 K.

views of only the liquid layer are also shown. From 400 ps on, more localized “dry” regions appear on the wall surface until at 600 ps several broad dry patches can be observed (this is clearly visible in the above-mentioned top views). The average thickness of the liquid region decreases to almost one third of the initial thickness at

700 ps. The evaporation continues until at 1000 ps only a few patches of liquid can be observed on the wall. Finally the entire liquid region disappears at about 1500 ps.

By plotting the density profiles at different times (Fig. 10), the variation of the liquid region near the wall can also be illustrated quite distinctly. From 0 to 300 ps, the position of the knee point that separates the liquid and gas regions changes very little, which implies that the average thickness of the liquid region changes very slowly and little vapor is produced in this period. However, from 300 ps on, there exists an apparent shifting of this turning point to the left, the average thickness of the liquid region is reduced, and evaporation is markedly faster. The evaporation process continues between 600 and 1500 ps, (Fig. 10(c)) until the thickness of the liquid region decreases gradually to zero.

Overall, at this lower wall temperature the vapor was formed locally near the heated wall and was gradually removed through the top surface of the layer. The dynamic lifting and floating of the liquid layer observed at high wall temperatures and discussed earlier was not a feature of the evaporation process this time.

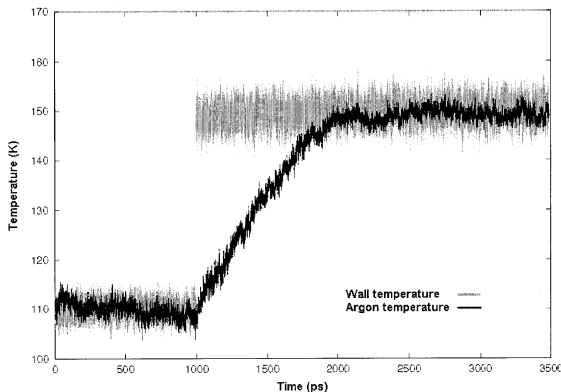


Fig. 8. Temperature history of wall and argon regions – low temperature case 150 K.

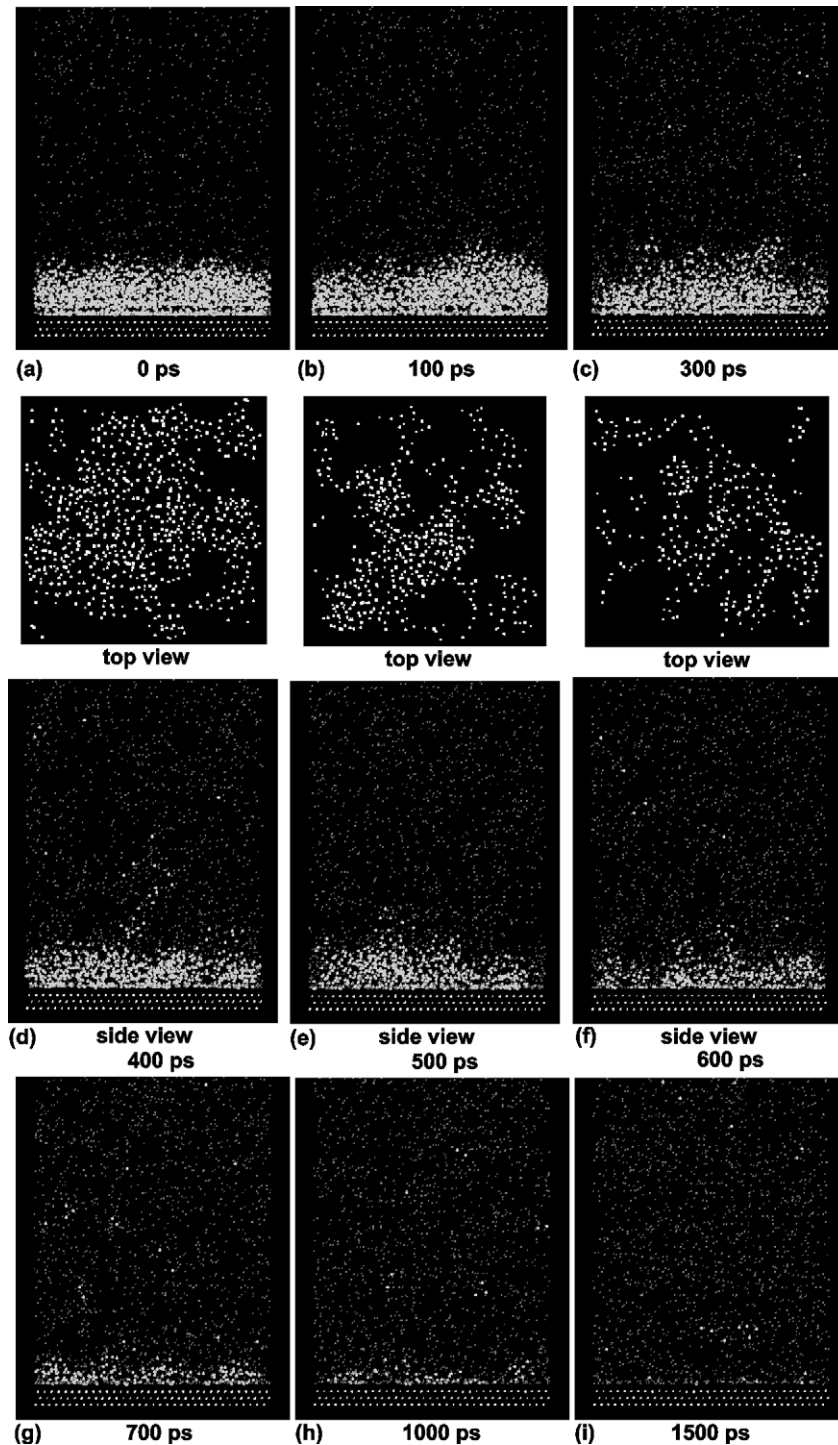


Fig. 9. Projection of the simulation domain in the  $y$ - $z$  plane at characteristic times – low temperature case 150 K.

When the new equilibrium state was established at 150 and 300 K after complete evaporation, we determined the velocity distribution of the argon atoms in

order to find out if they follow the Maxwellian curve [11]. We can see in Fig. 11 that although some fluctuations around the Maxwellian distribution are

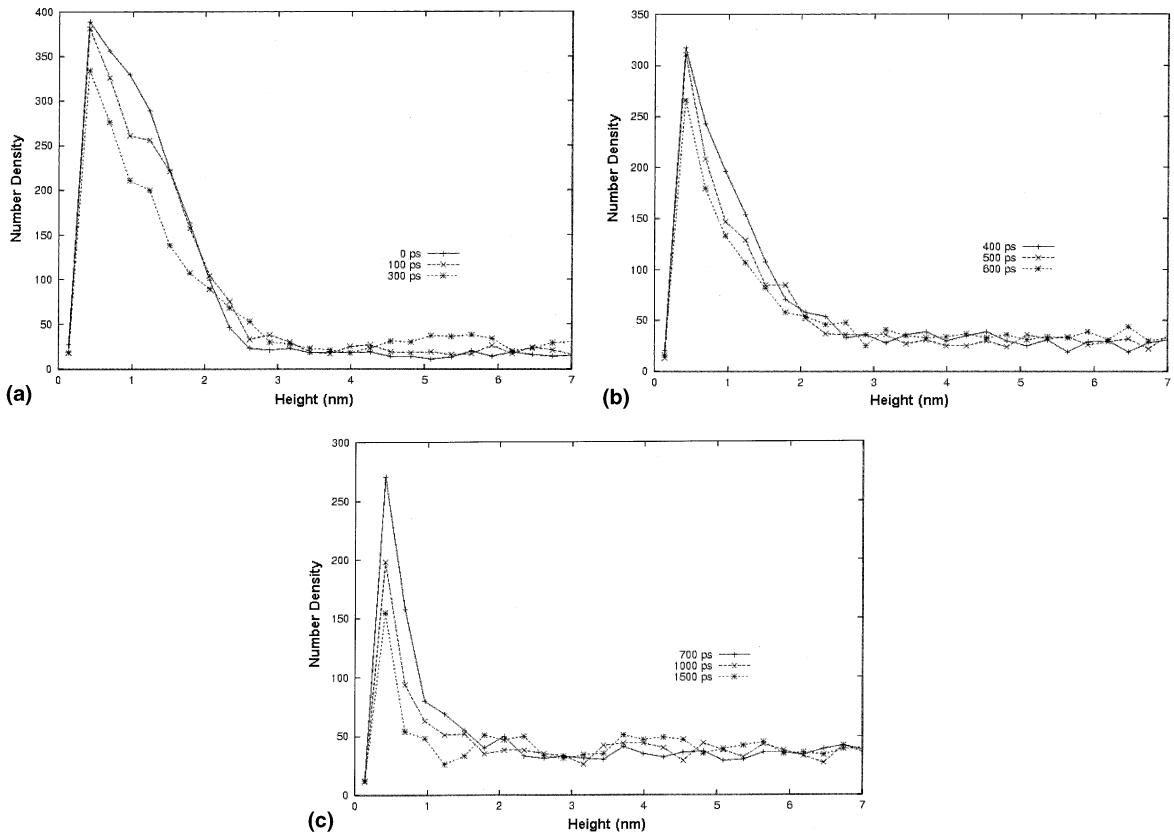


Fig. 10. Number density profiles at different times – low temperature case 150 K.

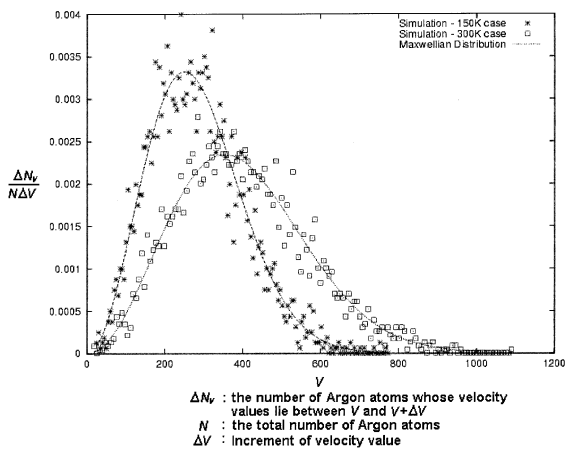


Fig. 11. Velocity distribution of the argon atoms at heat equilibrium after complete evaporation.

observed, the overall trend fits quite well the Maxwellian description, better so in the high temperature case of 300 K. This indicates that, as it should, in particular at higher temperatures, the velocity distri-

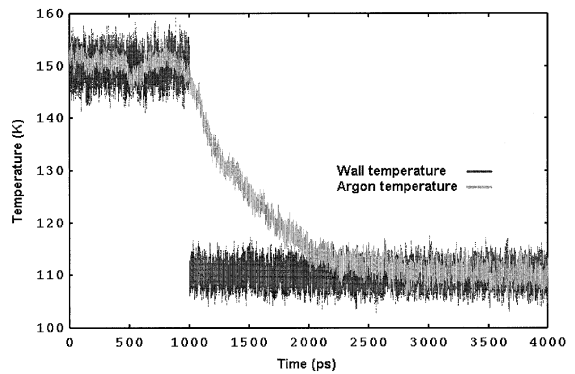


Fig. 12. Temperature history of the wall and argon regions – condensation case. Wall temperature 110 K.

bution of the atoms of argon gas is similar to that of an ideal gas.

### 5.3. Condensation

In addition to simulating the evaporation process, the capability of molecular dynamics simulations to describe

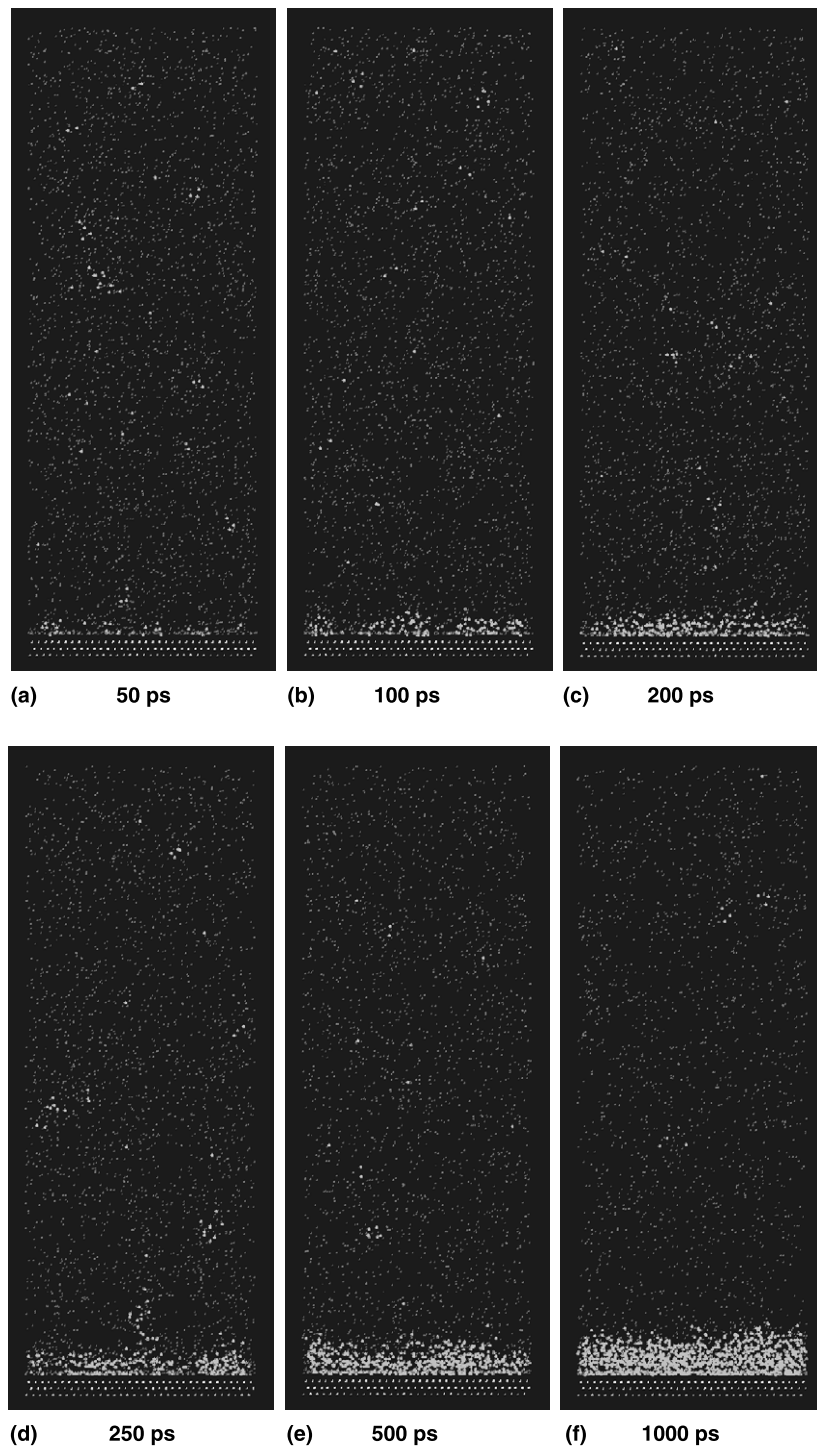


Fig. 13. Projection of the simulation domain in the  $y$ - $z$  plane at characteristic times of condensation. Wall temperature 110 K.

condensation was investigated. For this purpose, at the end of the process described earlier, after the entire liquid layer had evaporated and equilibrium had been reached, the wall temperature was suddenly reduced to 110 K.

Fig. 12 illustrates the temperature history of the simulation. We can see that the entire condensation process of the argon vapor lasted about 2500 ps, which is longer than the corresponding evaporation time.

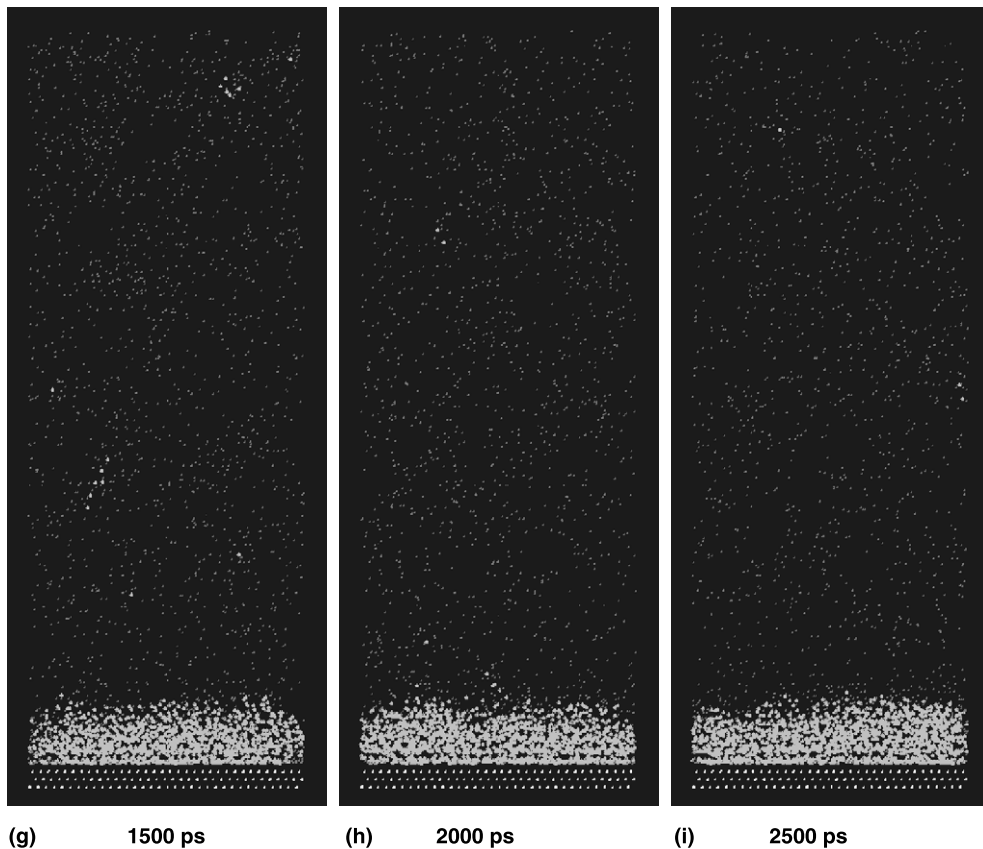


Fig. 13. (Continued)

Fig. 13 shows the projection of the entire simulation domain in the  $y$ - $z$  plane at different times of the simulation. At 50 ps (again we count the time from the beginning of the condensation procedure, when the temperature of the wall is suddenly reduced), we can see that several small regions of liquid appear to nucleate on the surface of the wall. Then at 100 ps larger liquid clusters form. These clusters gradually merge with one another so that at 200 ps a thin layer of liquid argon can be distinguished on the wall. Due to the heating from the hot vapor layer above, this thin liquid layer can temporarily break up at early times before it becomes stable (Fig. 13(d)). With the accumulation of condensed liquid, a stable layer of liquid argon forms at about 500 ps. From 500 to 1000 ps, the thickness of the liquid layer almost doubles. Subsequently there is a reduction of the condensation rate. From 1500 to 2500 ps, there is almost no visible variation on the thickness of liquid layer, which corresponds to the fact that the temperature difference between argon and wall decreases very slowly. In fact, we can see this tendency clearly from the gradual flattening of the temperature curve of argon from 1500 ps on (Fig. 12).

## 6. Conclusions

We investigated the vaporization phenomenon of an ultra-thin layer of liquid argon on a heated Platinum surface with molecular dynamics simulations.

Different vaporization behaviors were observed depending on the magnitude of the wall temperature (a moderately high temperature of 150 K and a markedly higher temperature of 300 K). Vaporization of liquid argon took place at the wall surface. The results reveal trends that agree with our knowledge of vaporization of a similar macroscopic system. For example, for high surface temperature, the vaporization process is reminiscent of the Leidenfrost phenomenon and after the formation of a vapor region between the surface and the liquid mass, the liquid deforms and floats acquiring an approximately spherical “droplet” shape as one would expect from macroscopic considerations. A more gradual evaporation process occurs at moderate wall temperatures. The simulations were extended to investigate condensation. After complete evaporation and upon reduction of the wall temperature, condensation takes place leading to reconstruction of the initial liquid layer.

### Acknowledgements

We wish to thank Prof. Maruyama of University of Tokyo for his detailed explanations of his earlier published results and for general fruitful discussions. We also wish to thank Prof. P. Koumoutsakos of ETH Zurich for fruitful discussions during the course of this work and for his insight regarding the efficiency of numerical methods pertinent to molecular dynamics simulations. This work was supported in part by the Swiss National Science Foundation under grant number 2100-052327.97/1.

### References

- [1] B.J. Alder, T.E. Wainwright, Phase transition of a hard sphere system, *J. Chem. Phys.* 27 (1957).
- [2] A. Rahman, Correlations in the motion of atoms in liquid argon, *Phys. Rev.* 136A (1964).
- [3] L.N. Long, M.M. Micci, B.C. Wong, Molecular dynamics simulations of droplet evaporation, *Comp. Phys. Commun.* (1996).
- [4] J.K. Little, Simulation of droplet evaporation in supercritical environments using parallel molecular dynamics, Ph.D thesis, Department of Aerospace Engineering, The Pennsylvania State University, 1996.
- [5] S. Maruyama, T. Kimura, A molecular dynamics simulation of a bubble nucleation on solid surface, in: *Proceedings of the 5th ASME–JSME Thermal Engineering Joint Conference*, San Diego, USA, 1999.
- [6] M.P. Allen, D.J. Tildesley, *Computer Simulation of Liquids*, Clarendon Press, Oxford, 1987.
- [7] S. Pfalzner, P. Gibbon, *Many-Body Tree Methods in Physics*, Cambridge University Press, New York, 1996.
- [8] S.D. Stoddard, P.J. Ford, Numerical experiments on the stochastic behaviour of a Lennard–Jones gas system, *Phys. Rev. A* 8 (1973).
- [9] J.C. Tully, Dynamics of gas–surface interactions: 3D generalized Langevin model applied to fcc and bcc surfaces, *J. Chem. Phys.* 73 (4) (1980).
- [10] V.A. Rabinovich, A.A. Vasserman, V.I. Nedostup, L.S. Veksler, *Thermophysical Properties of Neon, Argon, Krypton, and Xenon*, Hemisphere, Washington, DC, 1988.
- [11] J.B. Hudson, *Surface Science: an Introduction*, Wiley, New York, 1998.